Upcoming SBS program in Hall A

Andrew Puckett
University of Connecticut
Hall A/C Summer Workshop 2019
June 28, 2019

UCONN Jefferson Lab

Acknowledgements

- Support from US DOE, Office of Science, Office of Nuclear Physics, Award ID DE-SC0014230 (Early Career research program)
- SBS and Hall A Collaborations
- Additional support from Jefferson Lab and University of Connecticut

SBS Original Motivation, OR: Why are we still interested in pushing elastic FF measurements to yet higher Q^2, when the measurements are so difficult?

GEp/GMp polarization transfer data are among the most-cited JLab results

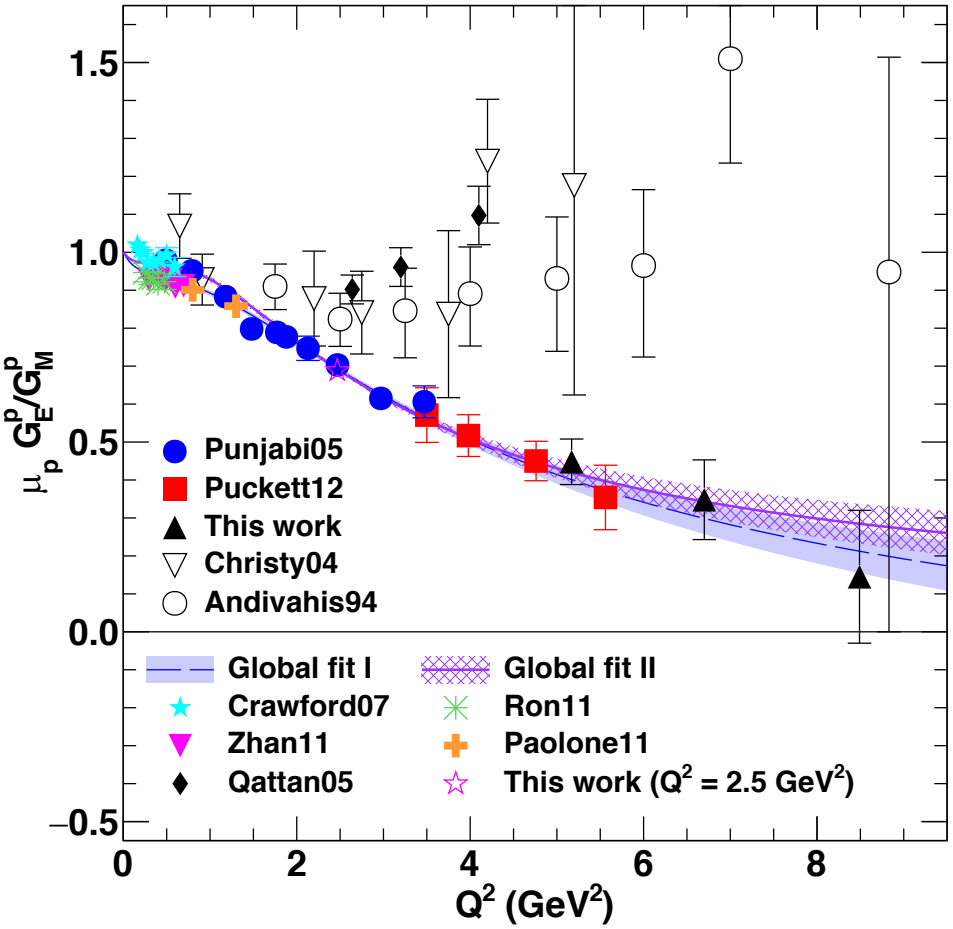

- GEp-I:
  - Jones *et al.,* **Phys. Rev. Lett. 84 (2000) 1398-1402: 855 INSPIRE-HEP citations**
  - Punjabi *et al.*, **Phys.Rev. C71 (2005) 055202: 418 INSPIRE-HEP citations**
- GEp-II:
  - Gayou *et al.*, **Phys.Rev.Lett. 88 (2002) 092301: 779 INSPIRE-HEP citations**
  - Puckett *et al.*, **Phys.Rev. C85 (2012) 045203: 130 INSPIRE-HEP citations**
- GEp-III/GEp-2γ:
  - Puckett *et al.*, **Phys.Rev.Lett. 104 (2010) 242301,** 244 INSPIRE-HEP citations
  - Meziane *et al.,* **Phys.Rev.Lett. 106 (2011) 132501,** 74 INSPIRE-HEP citations
  - Puckett *et al.*, **Phys.Rev. C96 (2017) no.5, 055203,** 13 INSPIRE-HEP citations
- Low-Q^2 data from JLab:
  - Ron *et al.*, **Phys.Rev.Lett. 99 (2007) 202002**, 69 INSPIRE-HEP citations
  - Ron *et al.*, **Phys.Rev. C84 (2011) 055204,** 91 INSPIRE-HEP citations
  - Zhan *et al.*, **Phys.Lett. B705 (2011) 59-64,** 163 INSPIRE-HEP citations
  - Paolone *et al.*, **Phys.Rev.Lett. 105 (2010) 072001**, 84 INSPIRE-HEP citations

High-Q^2 Nucleon Form Factors, GPDs and Spin

Flavor decomposition of nucleon EMFFs (neglecting strangeness):

$$F_{1,2}^{p} \approx e_u F_{1,2}^{u} + e_d F_{1,2}^{d}$$

$$F_{1,2}^{n} \approx e_u F_{1,2}^{d} + e_d F_{1,2}^{u}$$

Quark flavor FFs are integrals of valence quark GPDs H and E at zero skewness :

$$F_1^q(t) = \int_0^1 H_v^q(x,t)dx$$

$$F_2^q(t) = \int_0^1 E_v^q(x,t)dx$$

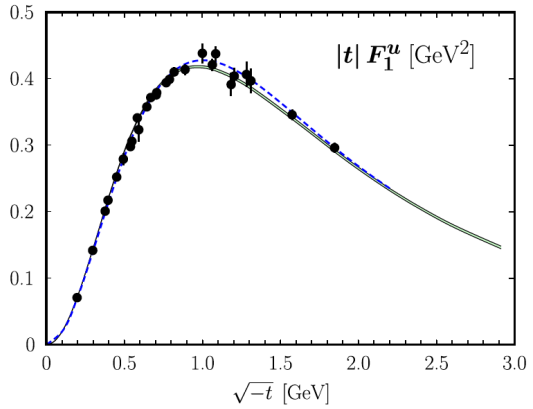

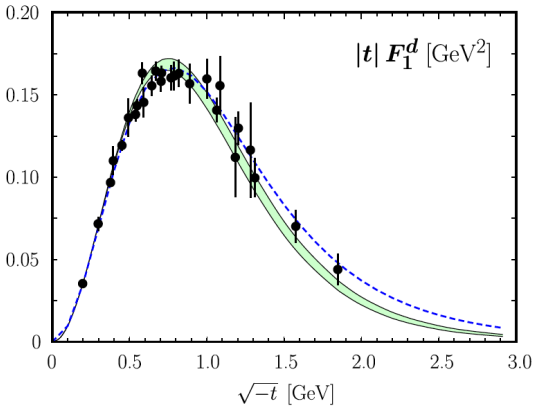

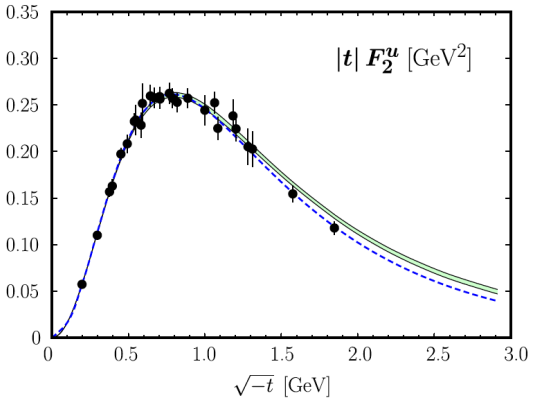

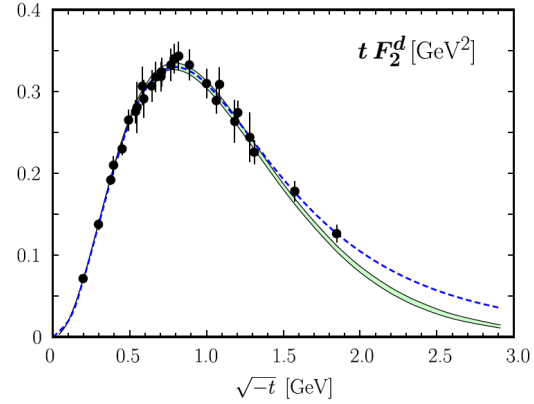

Phys.Rev.Lett. 78 (1997) 610-613: Ji sum rule for total angular momentum

$$J_q = \frac{1}{2}\int_{-1}^{+1} dx x[H^q(x,\xi,t=0) + E^q(x,\xi,t=0)].$$

Diehl, Kroll. Eur. Phys. J. C (2013) 73:2397

- FF data + forward PDFs from global DIS fits → model-dependent extraction of GPDs
- Compute valence-quark contributions to the Ji sum rule:

$$J_v^u = 0.230^{+0.009}_{-0.024}, \qquad J_v^d = -0.004^{+0.010}_{-0.016}$$

Continuum non-perturbative QCD and Dyson-Schwinger Equations—Exposing the dressed-quark mass function

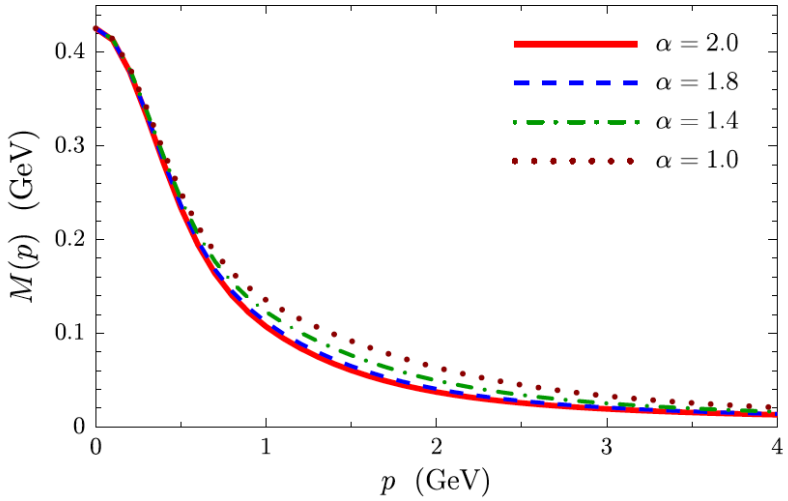

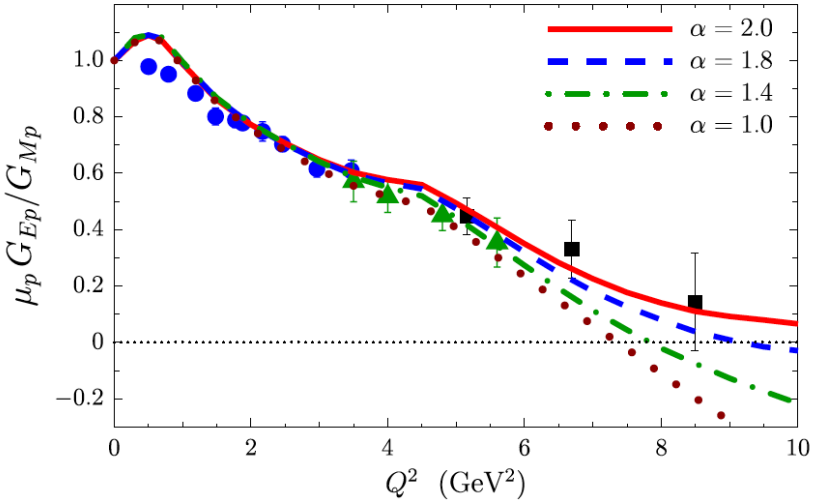

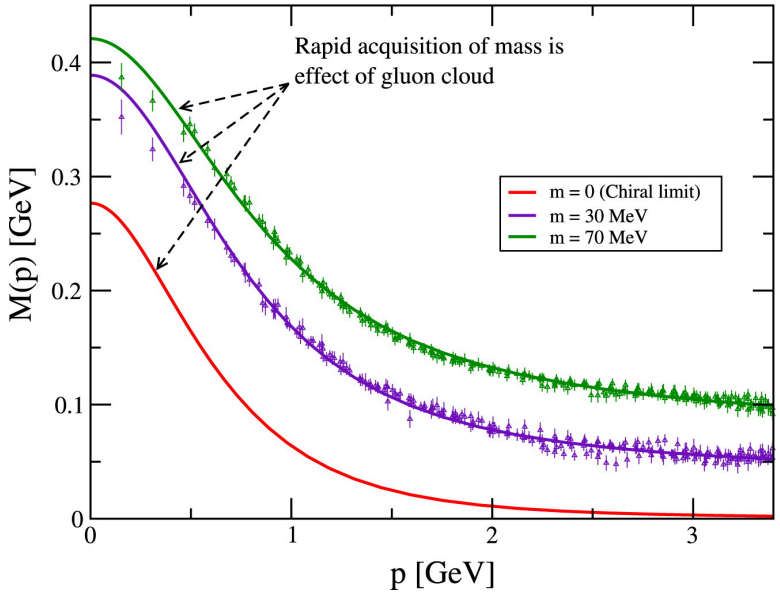

In the framework of Dyson-Schwinger equations, the high-Q^2 nucleon FFs ($Q^2 > 5$ GeV^2) are especially sensitive to momentum-dependent dressed-quark mass function in the few-GeV region, see e.g.,:

- I. Cloet, C. Roberts, A. Thomas: "Revealing Dressed Quarks via the Proton's Charge Distribution", **PRL 111, 101803 (2013)**
- I. Cloet and C. Roberts: "Explanation and Prediction of Observables Using Continuum Strong QCD", arxiv:1310.2651v2 (2013), **PPNP 77 (2014), 1-69**

Reaching high Q^2 in Lattice QCD

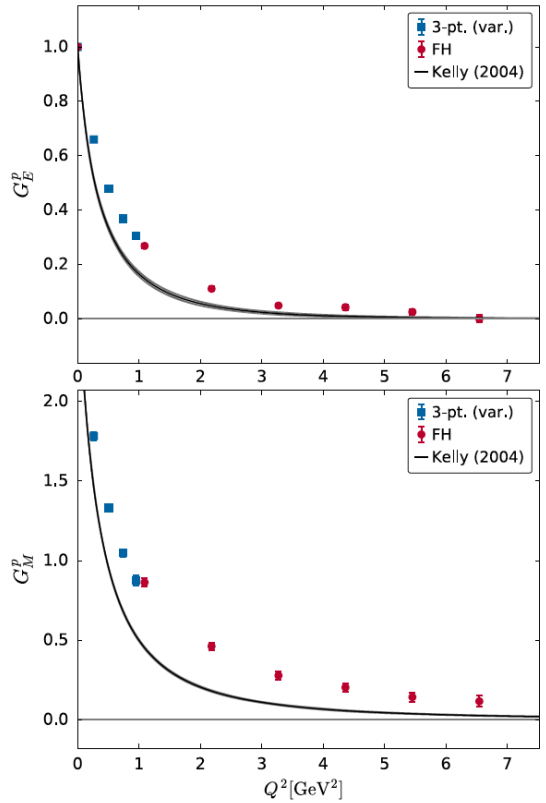

FIG. 3. G_E and G_M for the proton from the Feynman-Hellmann method and from a variational method described in Ref. [29] employed on the same ensemble. The experimental parametrization is from Ref. [49].

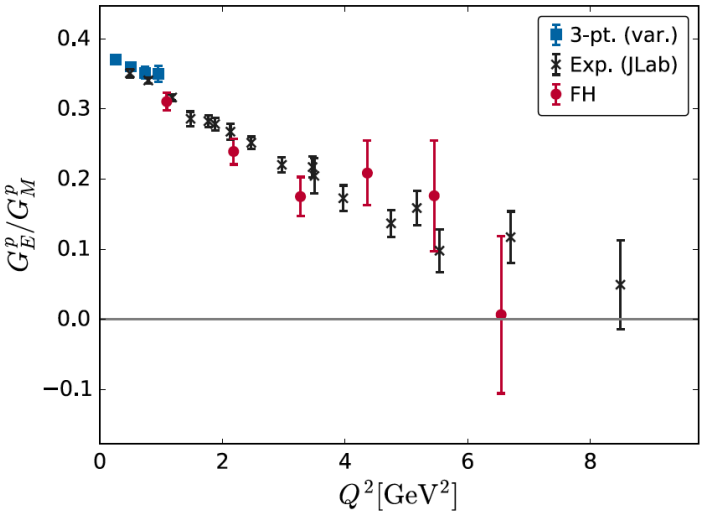

FIG. 4. Ratio G_E/G_M for the proton from the application of the Feynman-Hellmann method, from a variational analysis of three-point functions [29], and from experiment [5–7]. Note this is not scaled by the magnetic moment of the proton μ_p, as this would require phenomenological fits to the low-Q^2 data, which is not the focus of this work.

A. J. Chambers *et al.*, (QCDSF/UKQCD/CSSM Collaborations) Phys. Rev. D 96, 114509 (2017)

$$\frac{\partial E_\psi}{\partial \lambda} = \left\langle \psi \left| \frac{\partial H}{\partial \lambda} \right| \psi \right\rangle$$

- Novel application of the Feynman-Hellman method: relates hadronic matrix elements to energy shifts, allowing access to form factors via two-point correlators as opposed to more complicated three-point functions; improves signal-to-noise ratio for high-momentum states

Mapping the transverse densities and nucleon Imaging, II

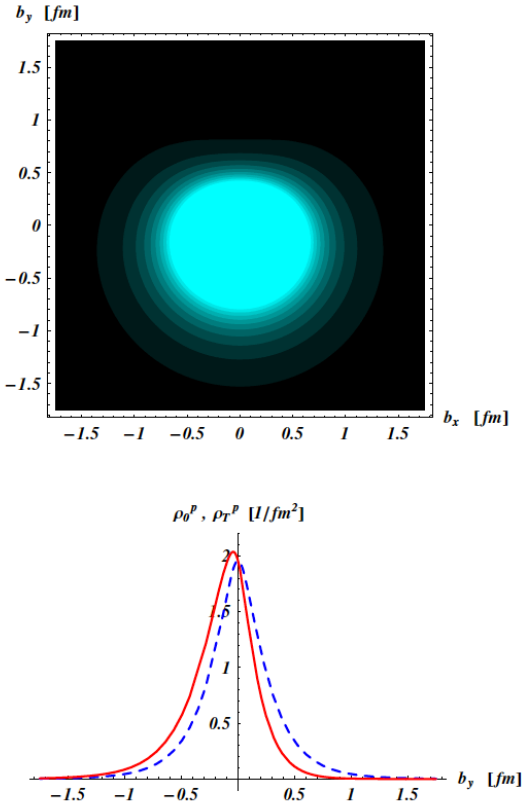

FIG. 1: Quark transverse charge densities in the *proton*. The upper panel shows the density in the transverse plane for a proton polarized along the x-axis. The light (dark) regions correspond with largest (smallest) values of the density. The lower panel compares the density along the y-axis for an unpolarized proton (dashed curve), and for a proton polarized along the x-axis (solid curve). For the proton e.m. FFs, we use the empirical parameterization of Arrington *et al.* [14].

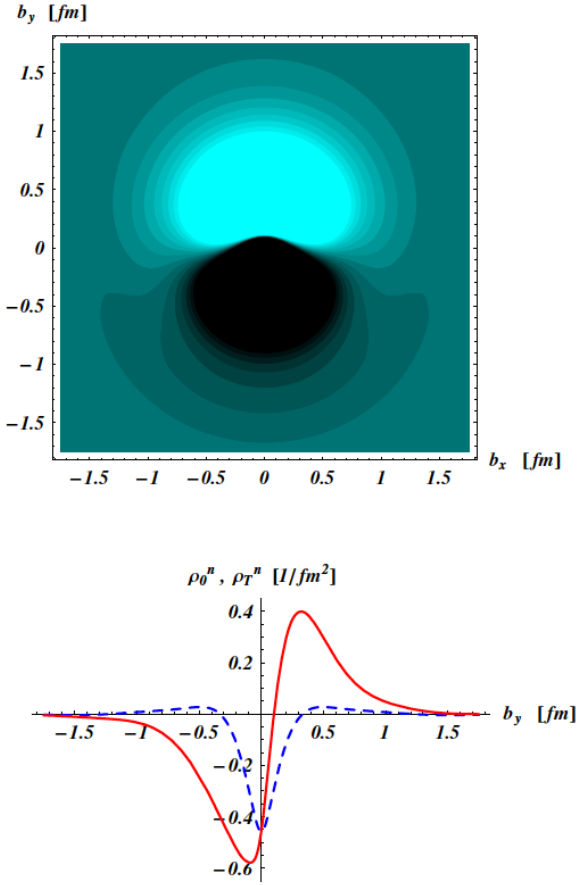

FIG. 2: Same as Fig. 1 for the quark transverse charge densities in the *neutron*. For the neutron e.m. FFs, we use the empirical parameterization of Bradford *et al.* [15].

Proton (left) and neutron (right) 2D polarized transverse charge densities from Carlson and Vanderhaeghen: Phys. Rev. Lett. 100, 032004 (2008)

Electron Scattering Kinematics @11 GeV

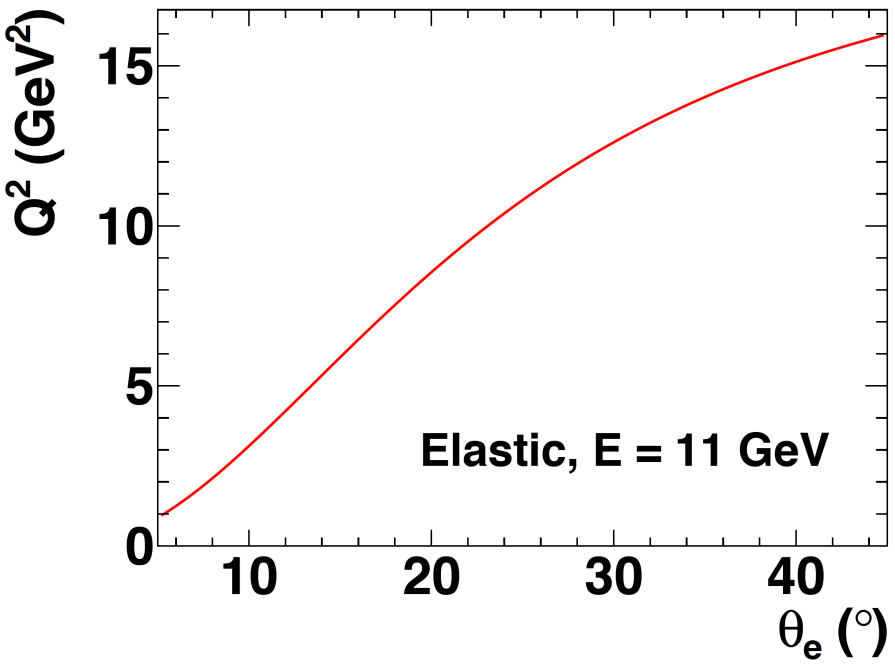

- Particles associated with the partonic (or other) degree of freedom that absorbed the virtual photon are found predominantly near the direction of the momentum transfer **q**
- ***Partonic interpretation of electron scattering data is accessible at large Q^2 → particles of interest are located at forward angles and high momentum***

- Measurements of elastic FFs, SIDIS, DVCS, etc involve coincidence N(e,e'X) (electroproduction) reactions, where X =
  - N' (elastic or quasi-elastic)
  - h (SIDIS or DVMP)
  - γ (DVCS)
- Virtual photon angle decreases as "inelasticity" increases:

$$Q^2 = 2M\nu x_{Bj}$$

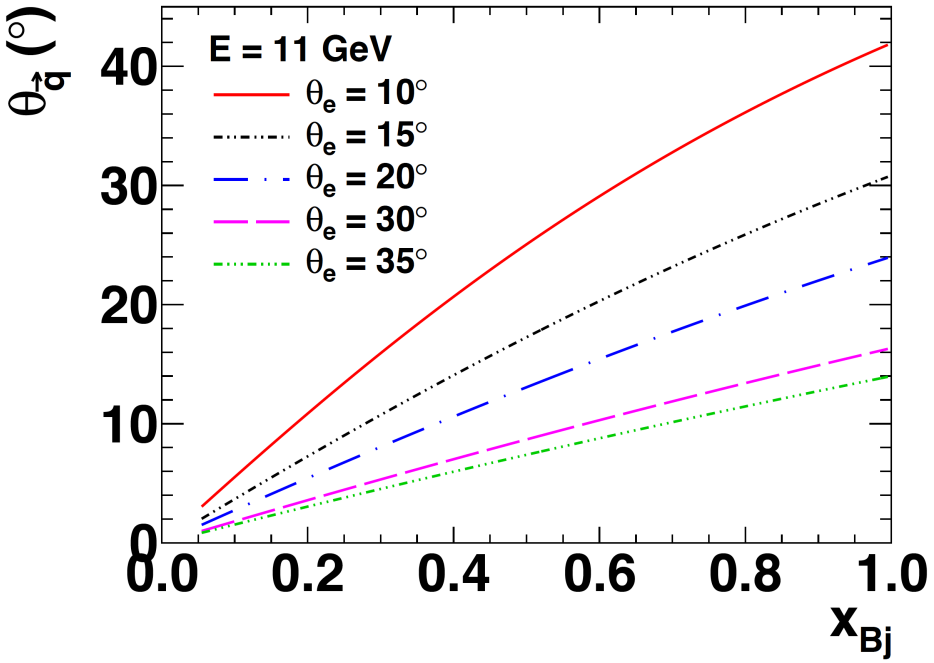

JLab detector landscape

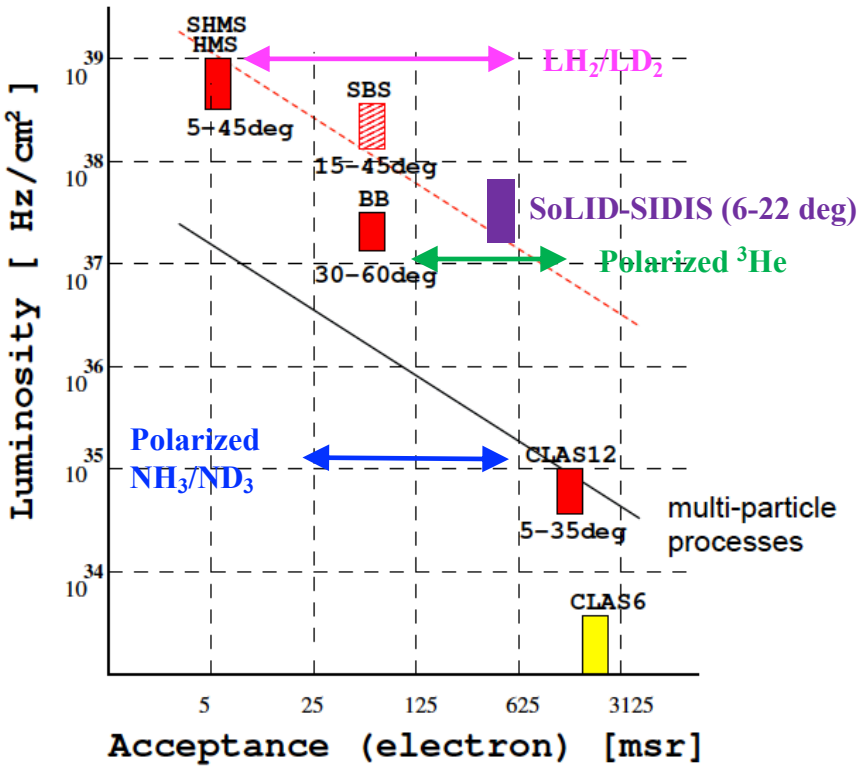

A range of 10^4 in luminosity.

A big range in solid angle:
from 5 msr (SHMS)
to about 1000 msr (CLAS12).

==========

The SBS is in the middle:
for solid angle (up to 70 msr)
and high luminosity capability.

In several A-rated experiments SBS was found to be the best match to the physics.

GEM allows a spectrometer with open geometry (->large acceptance) at high L.

- Complementary equipment/capabilities of Halls A, B, C allow optimal matching of (Luminosity x Acceptance) of the detectors to the luminosity capabilities of the targets, including state-of-the-art polarized target technology.

The Super BigBite Spectrometer in Hall A

Proton form factors ratio, GEp(5) (E12-07-109)

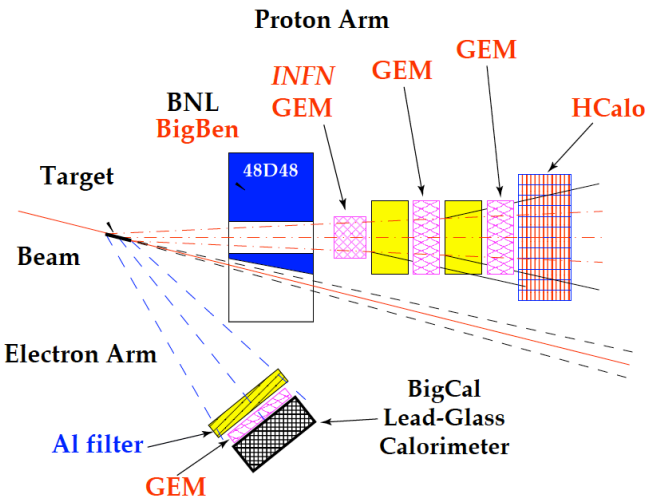

Neutron form factors, E12–09–016 and E12–09–019

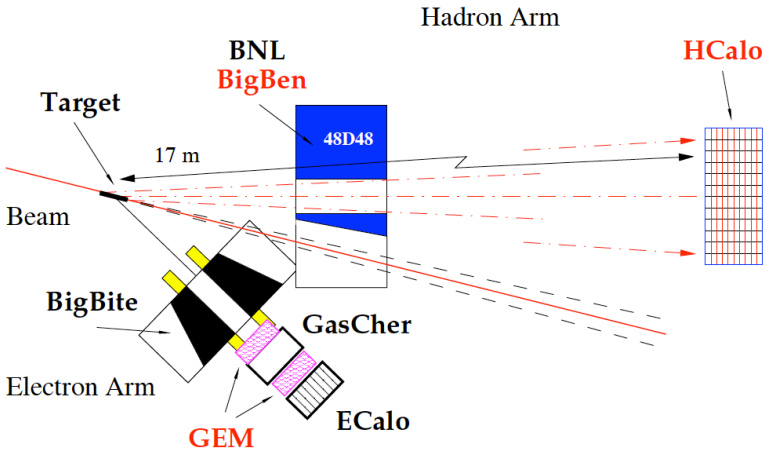

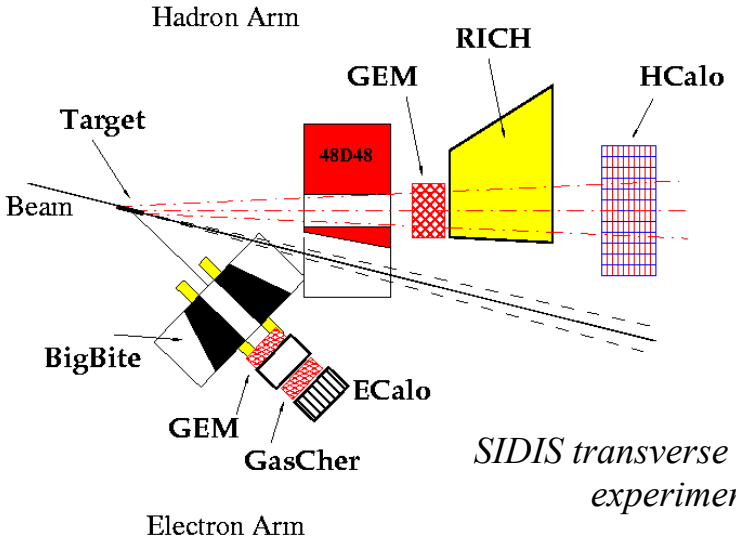

SIDIS transverse single-spin asymmetry experiment: E12-09-018

- What is SBS? → A 2.5 T*m dipole magnet with vertical bend, a cut in the yoke for passage of the beam pipe to reach forward scattering angles, and a flexible/modular configuration of detectors.
- Designed to operate at luminosities up to 10^{39} cm^{-2} s^{-1} with large momentum bite, moderate solid angle
- Time-tested "Detectors behind a dipole magnet", two-arm coincidence approach—historically most productive in fixed-target expts.
- ***Large solid-angle + high luminosity @ forward angles = most interesting physics!***

E12-09-019—Neutron Magnetic FF G_M^n to $Q^2 = 13.5\ GeV^2$

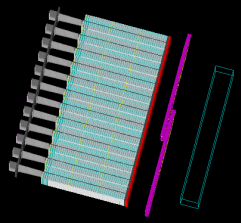

First SBS experiment: JLab Experimental Readiness Review (ERR) completed 2017, projected installation/start of SBS program in 2020

Neutron/proton Arm: SBS dipole, HCAL, and coordinate detector (not shown) for charged-particle veto

10-cm liquid deuterium/hydrogen target (luminosity ~ 2 × 10^{38})

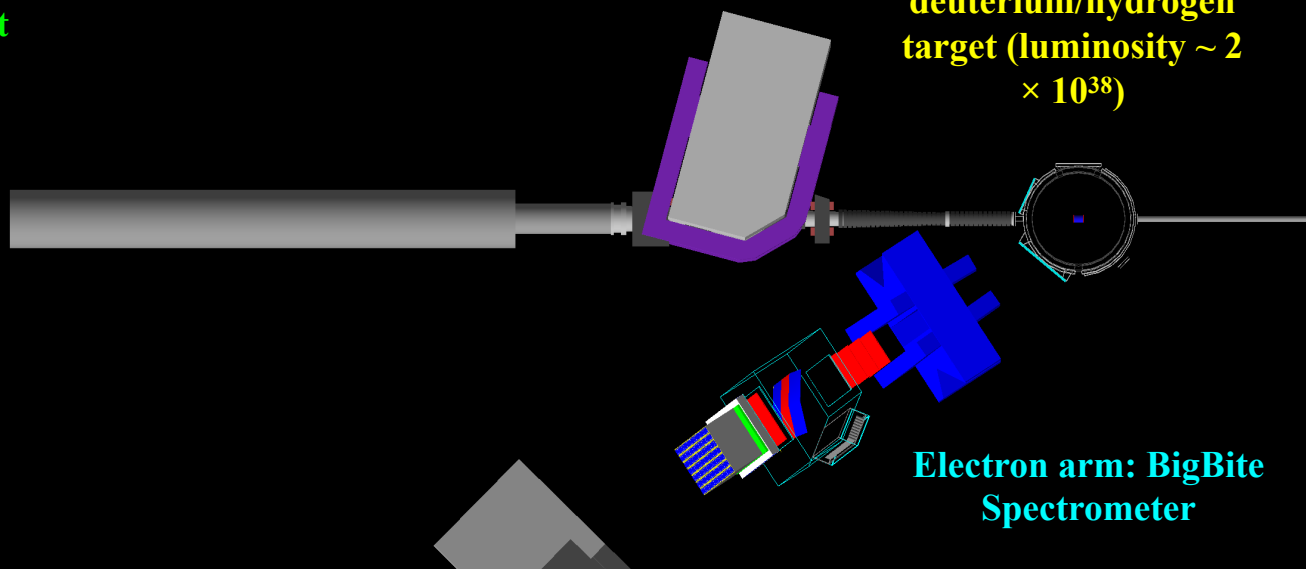

Electron arm: BigBite Spectrometer

- Neutron magnetic form factor at large Q^2 is obtained from the ratio of quasi-elastic d(e,e'n)p/d(e,e'p)n cross sections on a deuterium target and precise knowledge of elastic ep cross section
- SBS dipole deflects protons to separate from neutrons (relative to $\vec{q}$ vector); nucleon momentum is measured using time-of-flight method to separate quasi-elastic/inelastic channels.
- Existing BigBite spectrometer with upgraded detector package detects the scattered electron.

SBS G_{Mn} projected Results

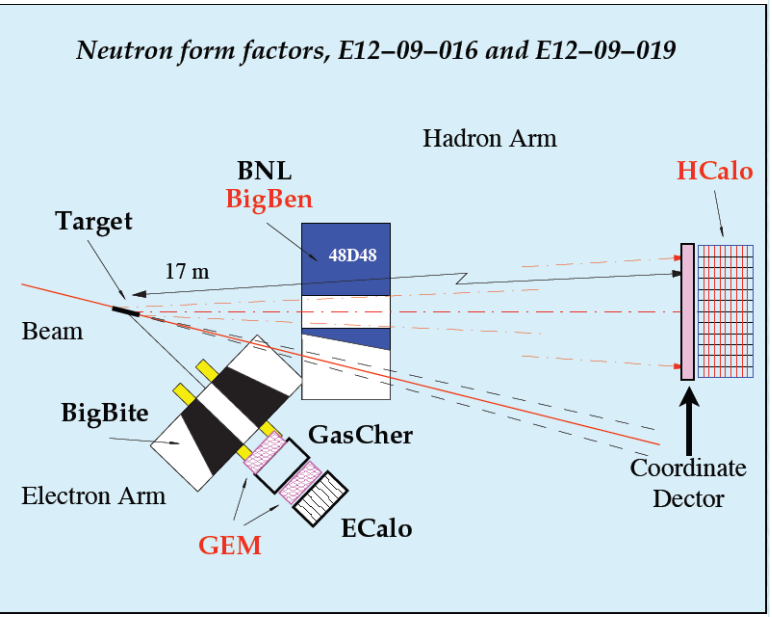

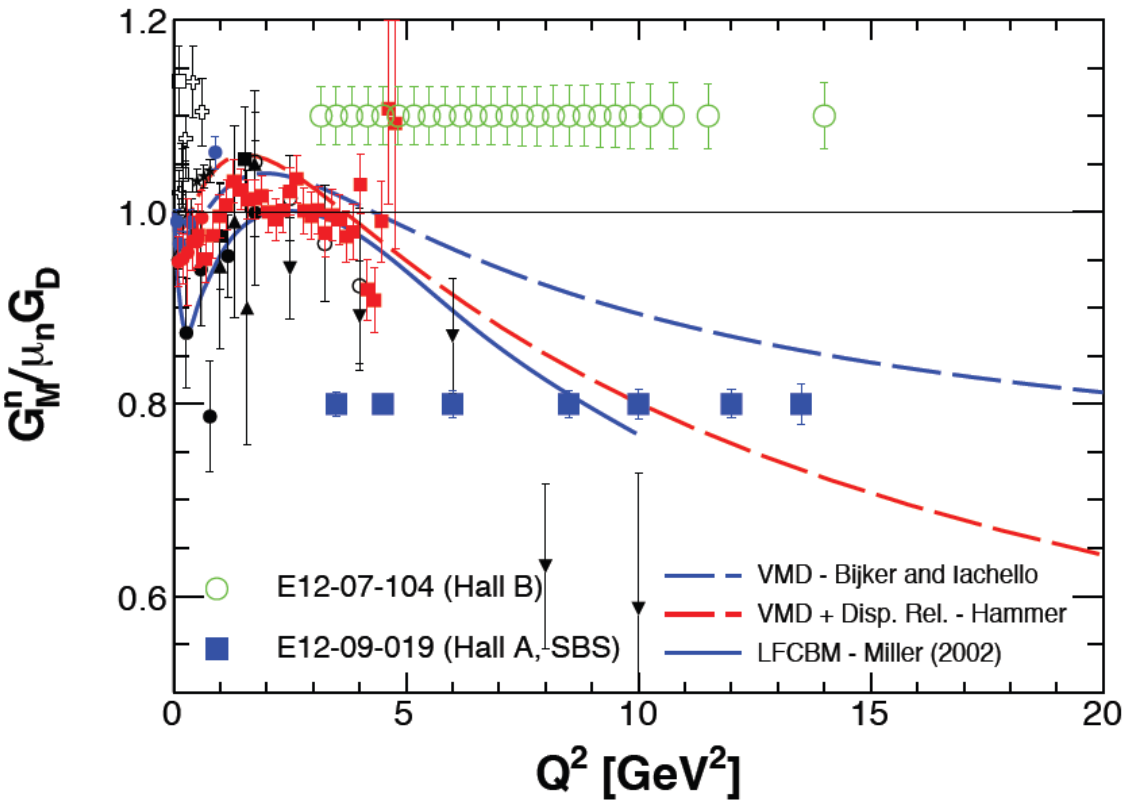

- SBS as neutron arm w/48D48 + HCAL
- Magnet deflects protons to separate from neutrons
- BigBite as electron arm w/upgraded 12 GeV detector package (including re-use of GEMs, built for GEP, not otherwise in use during BigBite expt's.)
- Standard LH2/LD2 target
- Different detection method—different (and smaller) systematics; complementary to CLAS12 G_{Mn} measurement
  - Overlapping collaborations between CLAS12 and SBS experiments.

GEN via Recoil Polarization—E12-17-004

Recoil Neutron Polarimetry at High Momentum

- Until recently no data on n+C→n+p+X at several GeV/c (nor any nucleus)

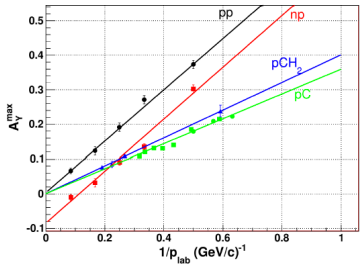

- A_y for np→np falling rapidly with increasing neutron momentum
- A_y for charge-exchange np→pn large at sufficiently large t (θ_p ~ few deg.)
- $\sigma_{np\to np}$ factor ~10 higher than $\sigma_{np\to pn}$

Diebold et al., PRL 35,(1975),632
Fits: Ladygin JINR
E13-99-123 (1999)

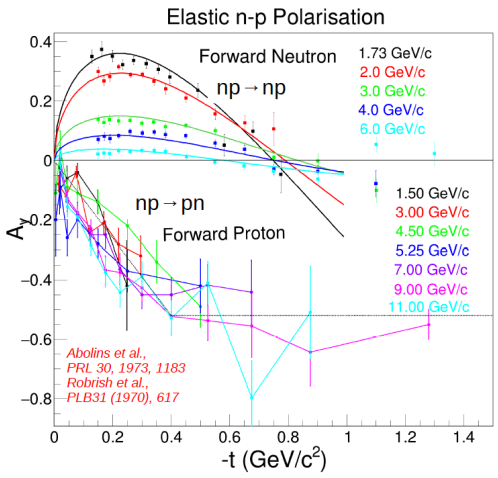

Abolins et al., PRL 30, 1973, 1183
Robrish et al., PLB31 (1970), 617

GEn-Recoil Experimental Layout

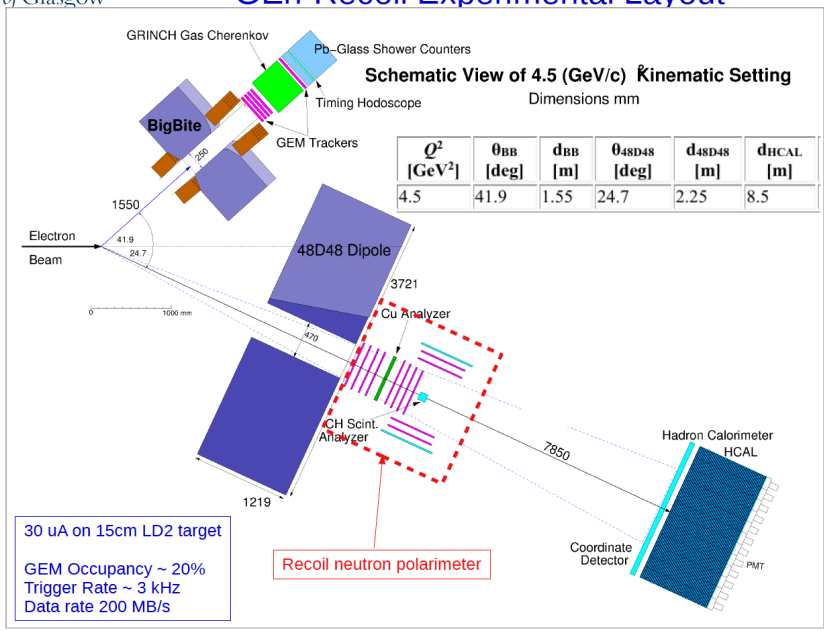

Q^2 [GeV^2]	θ_{BB} [deg]	d_{BB} [m]	θ_{48D48} [deg]	d_{48D48} [m]	d_{HCAL} [m]
4.5	41.9	1.55	24.7	2.25	8.5

30 uA on 15cm LD2 target

GEM Occupancy ~ 20%
Trigger Rate ~ 3 kHz
Data rate 200 MB/s

E12-17-004 Projected Results

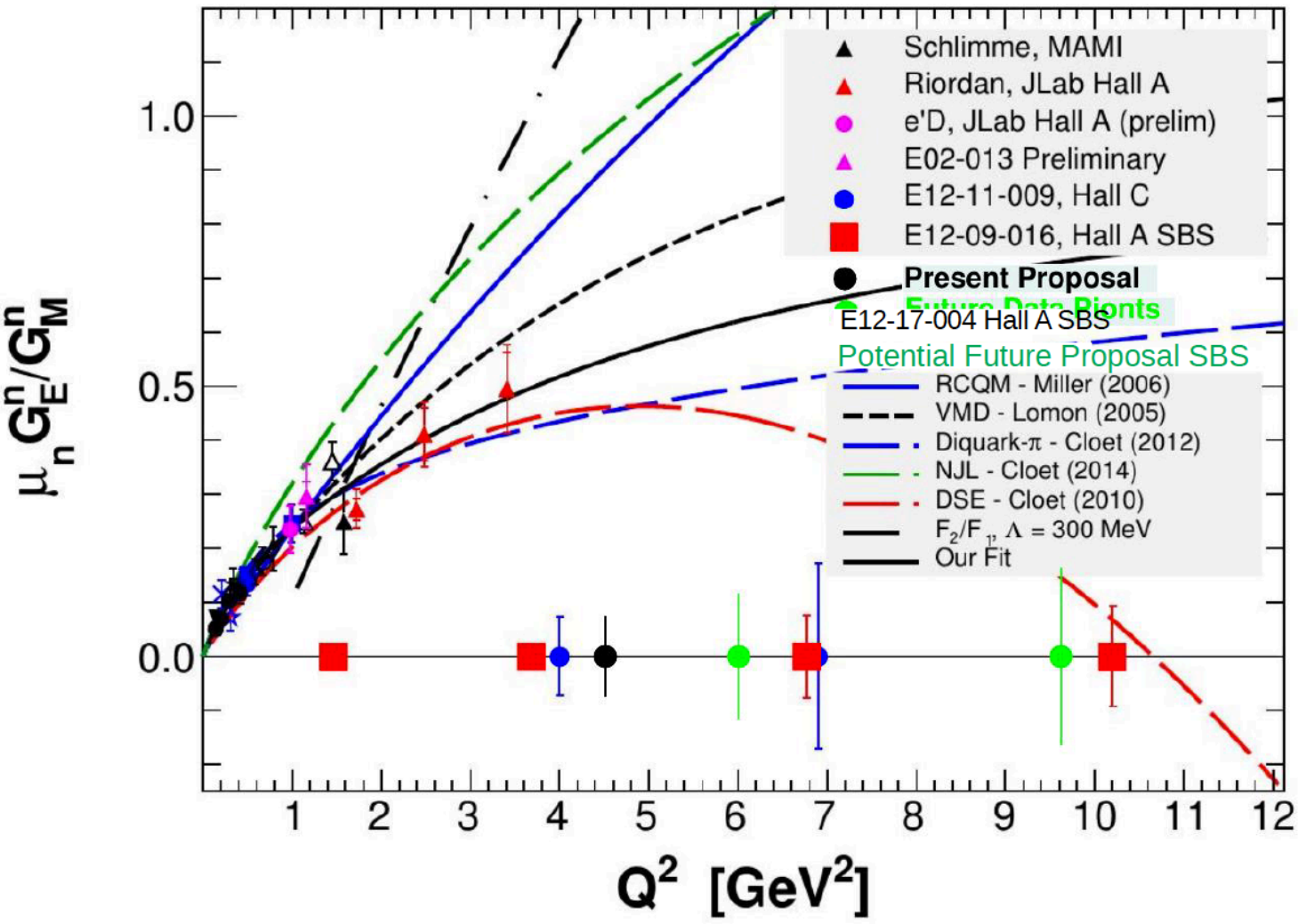

Experiment E12-09-016 (G_{En} at large Q^2)

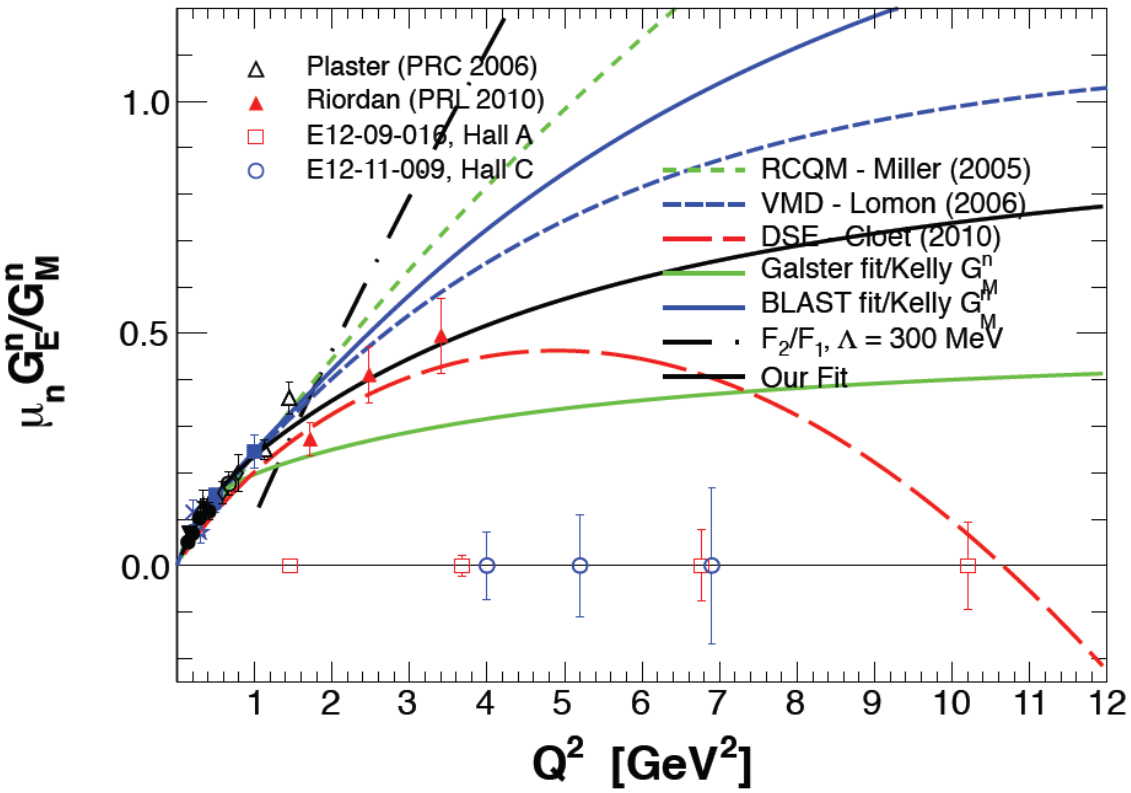

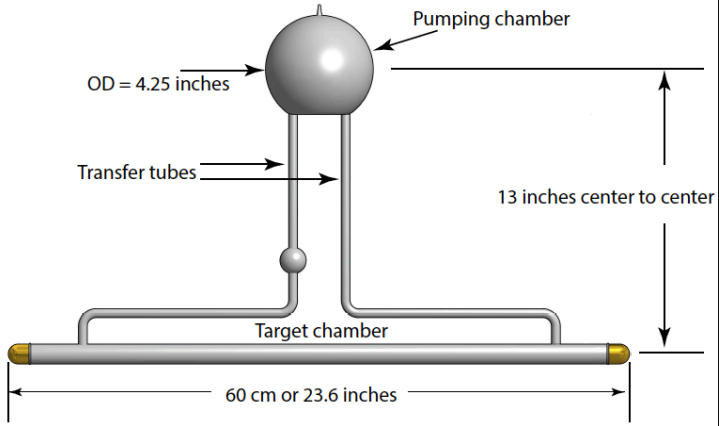

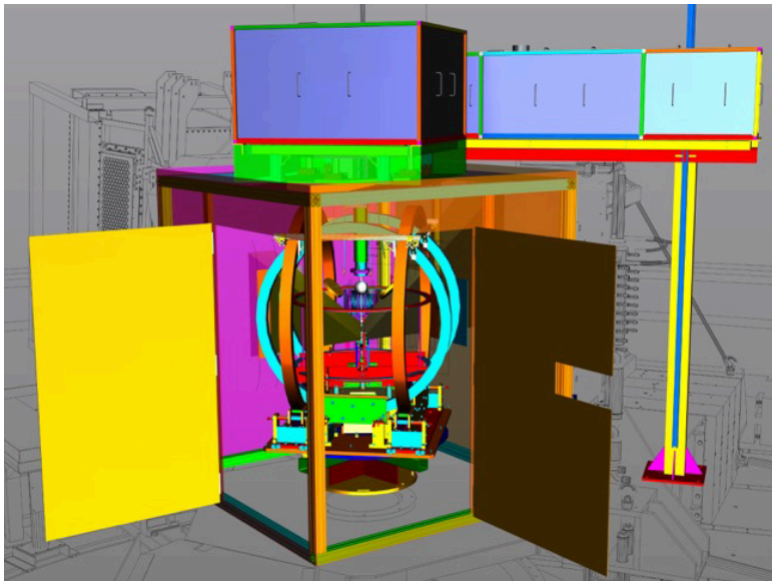

Conceptual and Engineering Designs of Polarized ^{3}He target

- Detector configuration same as GMN experiment
- Upgraded, high-luminosity polarized ^{3}He target based on spin-exchange optical pumping and convection-driven circulation of polarized gas between optical pumping chamber and target chamber.
- Will reach Q^2 = 10 GeV^2 in 50 days (approximately tripling Q^2 reach of the data)

Experiment E12-07-109 (G_{Ep}/G_{Mp} at large Q^2)

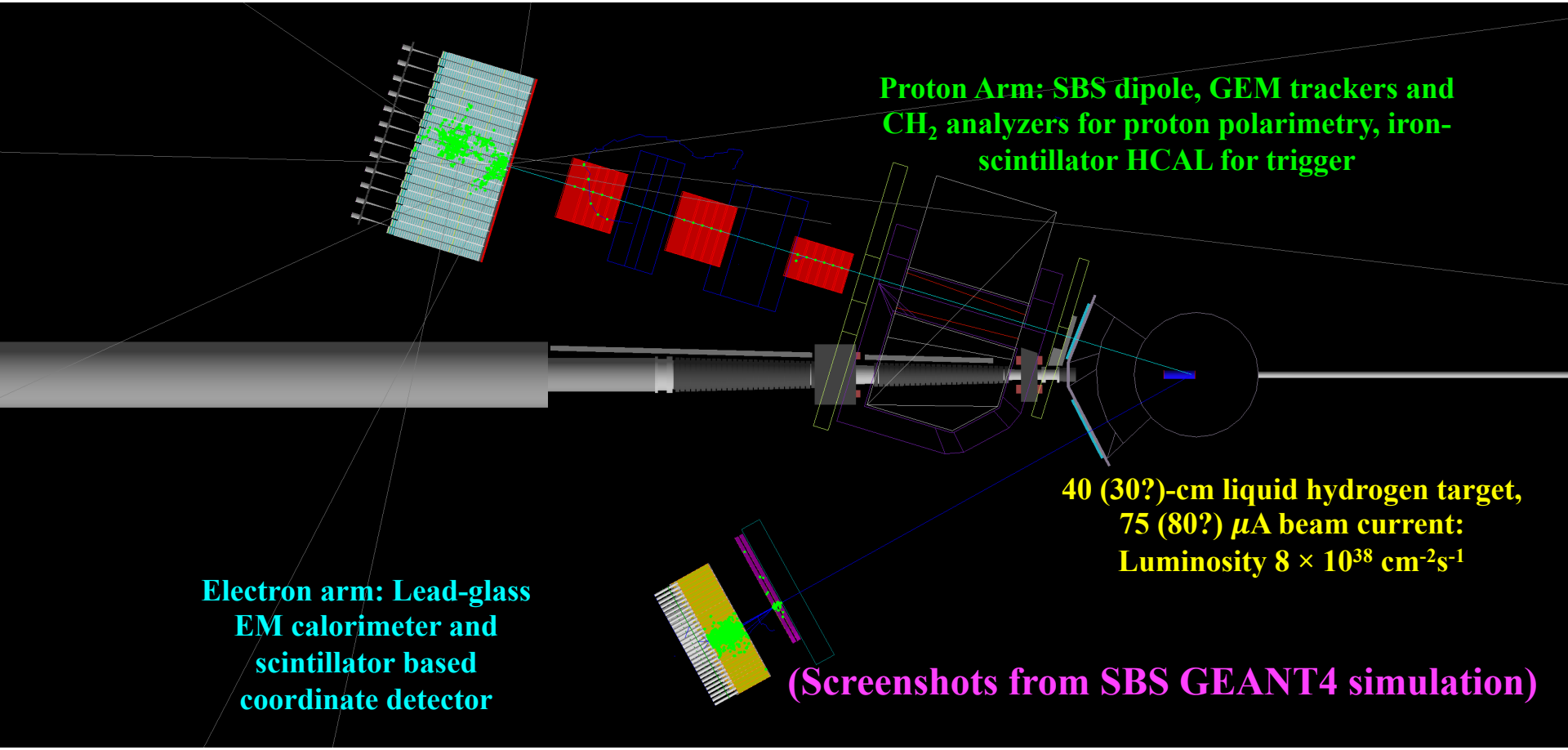

- Original motivation for SBS concept. Need large solid angle to overcome rapidly falling cross section at large Q^2 in elastic *ep* scattering. New double proton polarimeter with GEM-based tracking and hadronic calorimeter-based trigger
- Lead-glass electromagnetic calorimeter to detect the scattered electron in coincidence (using two-body kinematic correlations to aid tracking in high-rate environment and reject inelastic background events); also provides a selective trigger for high-energy electrons.

SBS G_E^p Projected Results

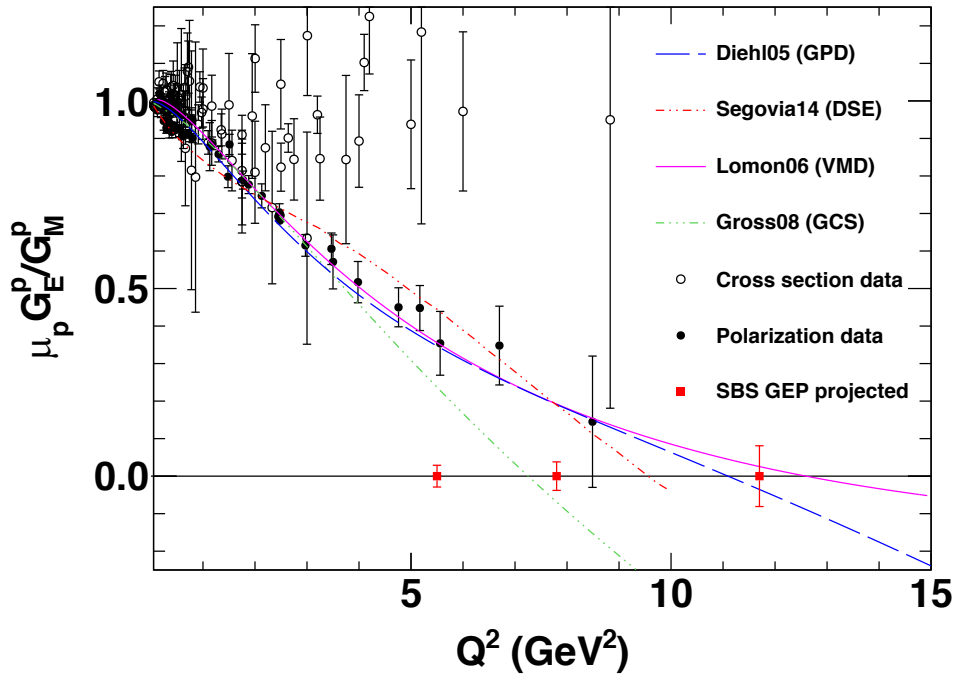

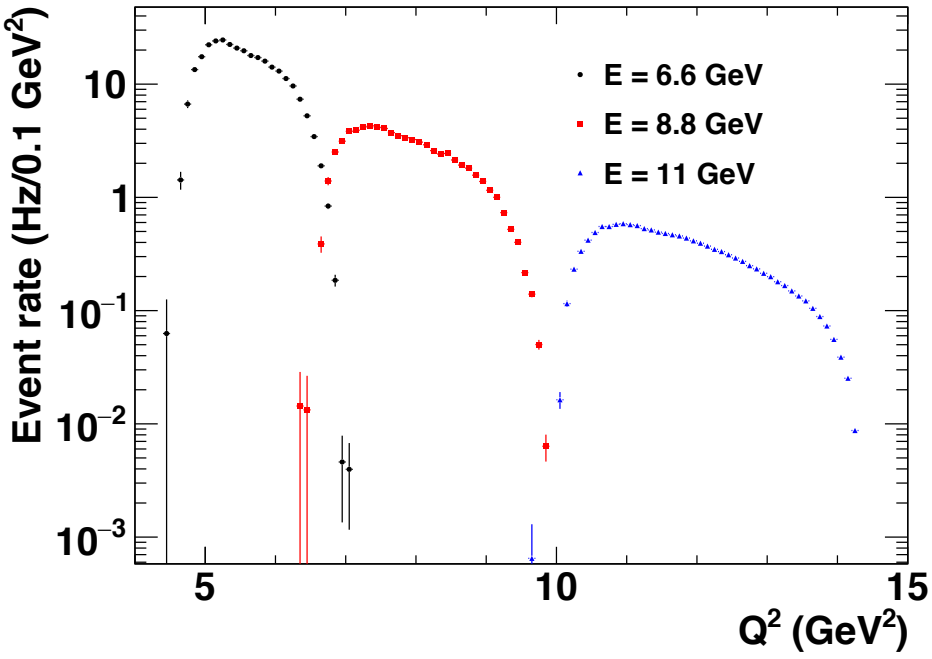

Jeopardy update submitted to PAC47!

TABLE I. Kinematics, projected accuracy and beam time allocations. The projected statistical uncertainties in the form factor ratio include the assumption of 70% overall event reconstruction efficiency due to the combined efficiencies of the individual detectors, including DAQ dead-time.

E_{beam}, GeV	Q^2 range, GeV^2	$\langle Q^2 \rangle$ GeV^2	θ_{ECAL} degrees	$\langle E'_e \rangle$, GeV	θ_{SBS} degrees	$\langle P_p \rangle$ GeV	$\langle \sin\chi \rangle$ degrees	Event rate Hz	Days	$\Delta(\mu G_E/G_M)$
6.6	4.5-7.0	5.5	29.0	3.66	25.7	3.77	0.72	291	2	0.029
8.8	6.5-10.0	7.8	26.7	4.64	22.1	5.01	0.84	72	11	0.038
11.0	10.0-14.5	11.7	29.0	4.79	16.9	7.08	0.99	13	32	0.081

SBS Form Factor Program–Summary

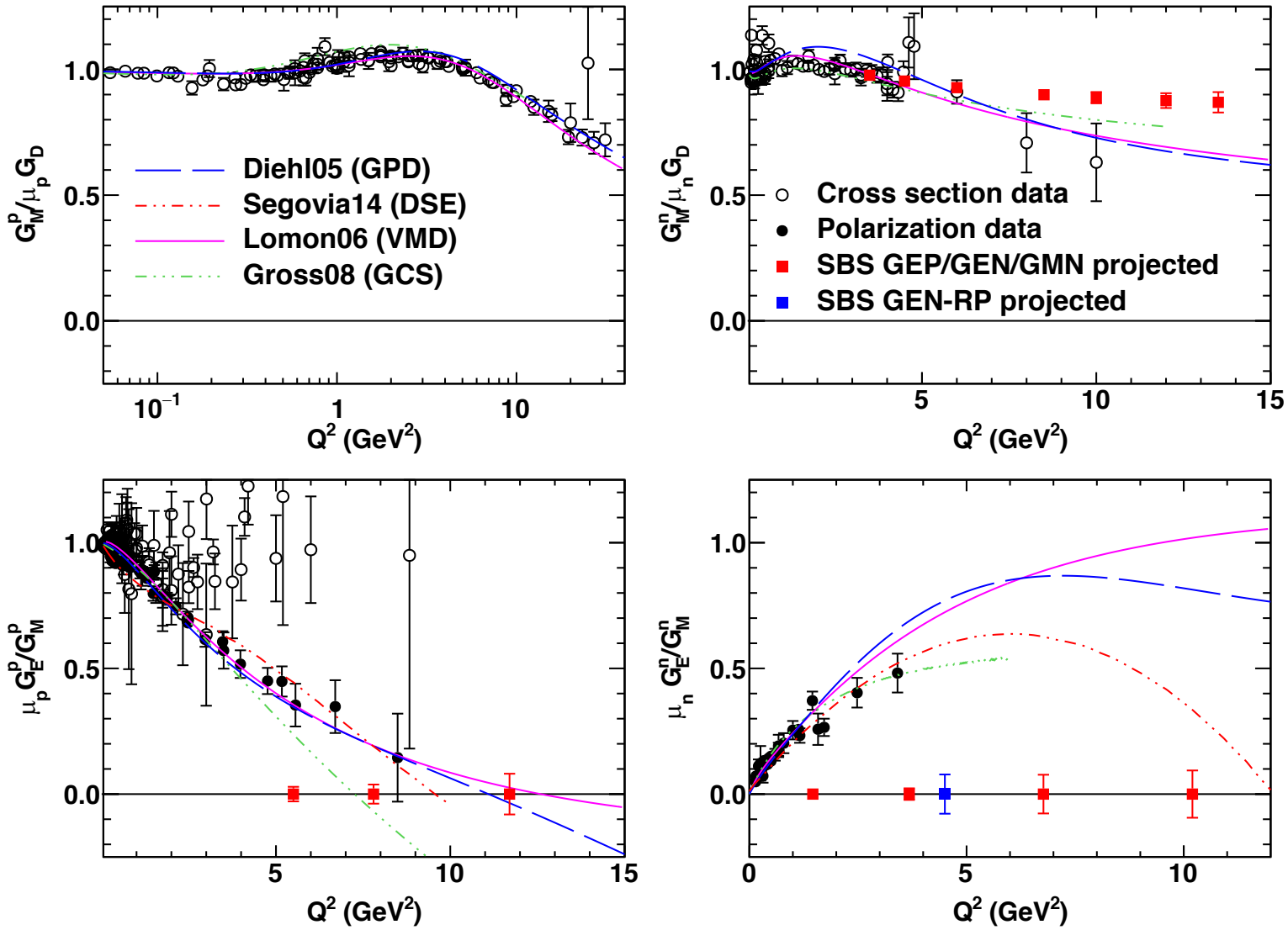

Semi-Inclusive Deep Inelastic Scattering

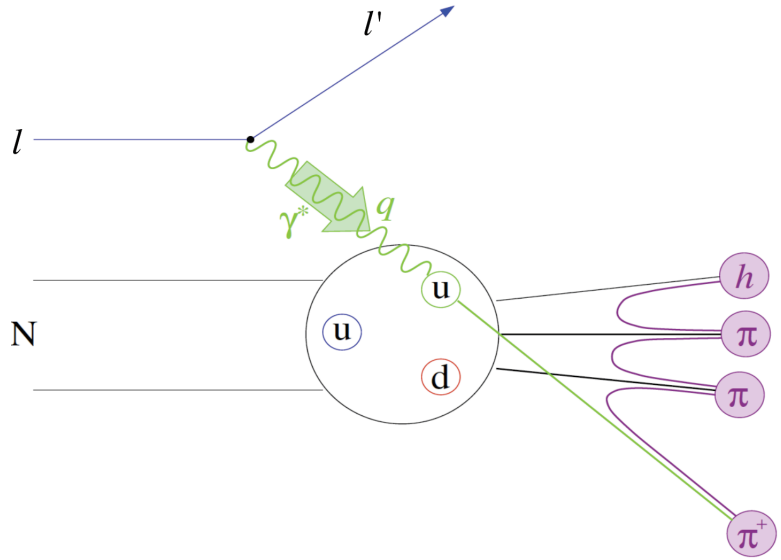

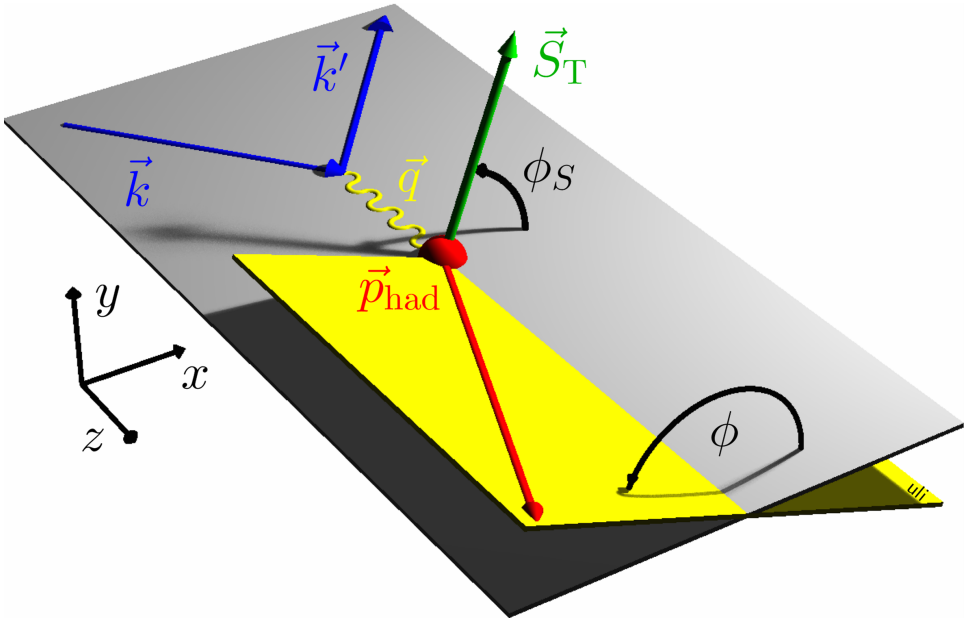

• Detecting leading (high-energy) hadrons in DIS, N(e,e'h)X provides sensitivity to additional aspects of the nucleon's partonic structure not accessible in inclusive DIS:

- quark flavor
- quark transverse motion
- quark transverse spin

• Goal of SIDIS studies is (spin-correlated) 3D imaging of nucleon's quark structure in momentum space.

• Transverse Momentum Dependent (TMD) PDF formalism: ***Bacchetta et al. JHEP 02 (2007) 093, Boer and Mulders, PRD 57, 5780 (1998), etc, etc...***

Transverse target spin effects in SIDIS

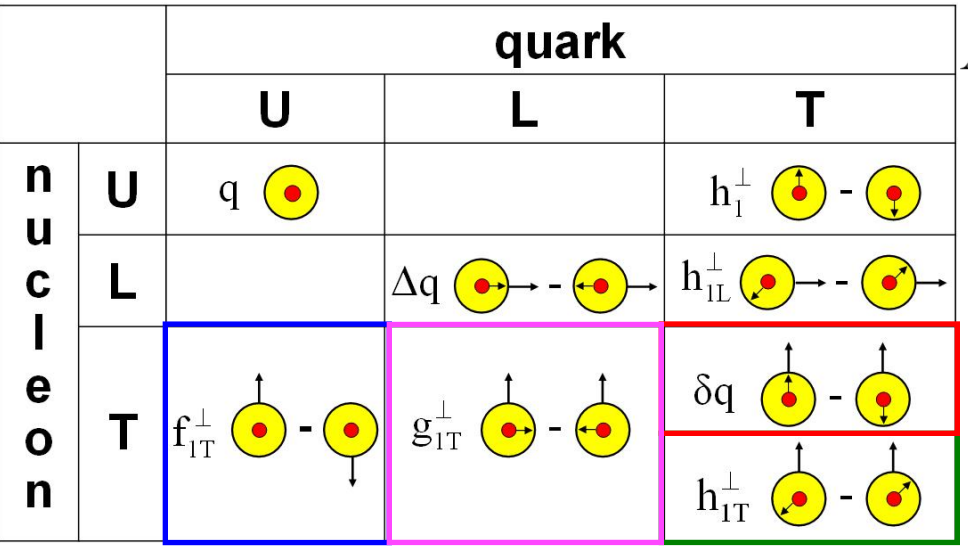

Transverse target spin-dependent cross section for SIDIS

- Collins effect—chiral-odd quark transversity DF; chiral-odd Collins FF
- Sivers effect—access to quark OAM and QCD FSI mechanism
- "Transversal helicity" g_{1T}—real part of S wave-P wave interference (Sivers = imaginary part) (requires polarized beam)
- "Pretzelosity" or Mulders-Tangerman function—interference of wavefunction components differing by 2 units of OAM

$$A_{UT}(\phi,\phi_S) = \frac{1}{P_T}\frac{d\sigma(\phi,\phi_S)-d\sigma(\phi,\phi_S+\pi)}{d\sigma(\phi,\phi_S)+d\sigma(\phi,\phi_S+\pi)}$$
$$= A_{UT}^{Collins}\sin(\phi+\phi_S) + A_{UT}^{Sivers}\sin(\phi-\phi_S) + A_{UT}^{Pretz}\sin(3\phi-\phi_S)$$

$$A_{UT}^{Collins} \propto \delta q \otimes H_1^\perp$$
$$A_{UT}^{Sivers} \propto f_{1T}^\perp \otimes D_1$$
$$A_{UT}^{Pretz} \propto h_{1T}^\perp \otimes H_1^\perp$$

D_1 = unpolarized fragmentation function

$H_1^\perp$ = Collins fragmentation function

$$A_{LT}(\phi,\phi_S) = \frac{1}{P_e P_T}\frac{Y_+(\phi,\phi_S)-Y_-(\phi,\phi_S)}{Y_+(\phi,\phi_S)+Y_-(\phi,\phi_S)}$$
$$\sim A_{LT}^{\cos(\phi-\phi_S)}\cos(\phi-\phi_S)$$
$$\sim g_{1T}\otimes D_1$$

E12-09-018—Transversely Polarized SIDIS

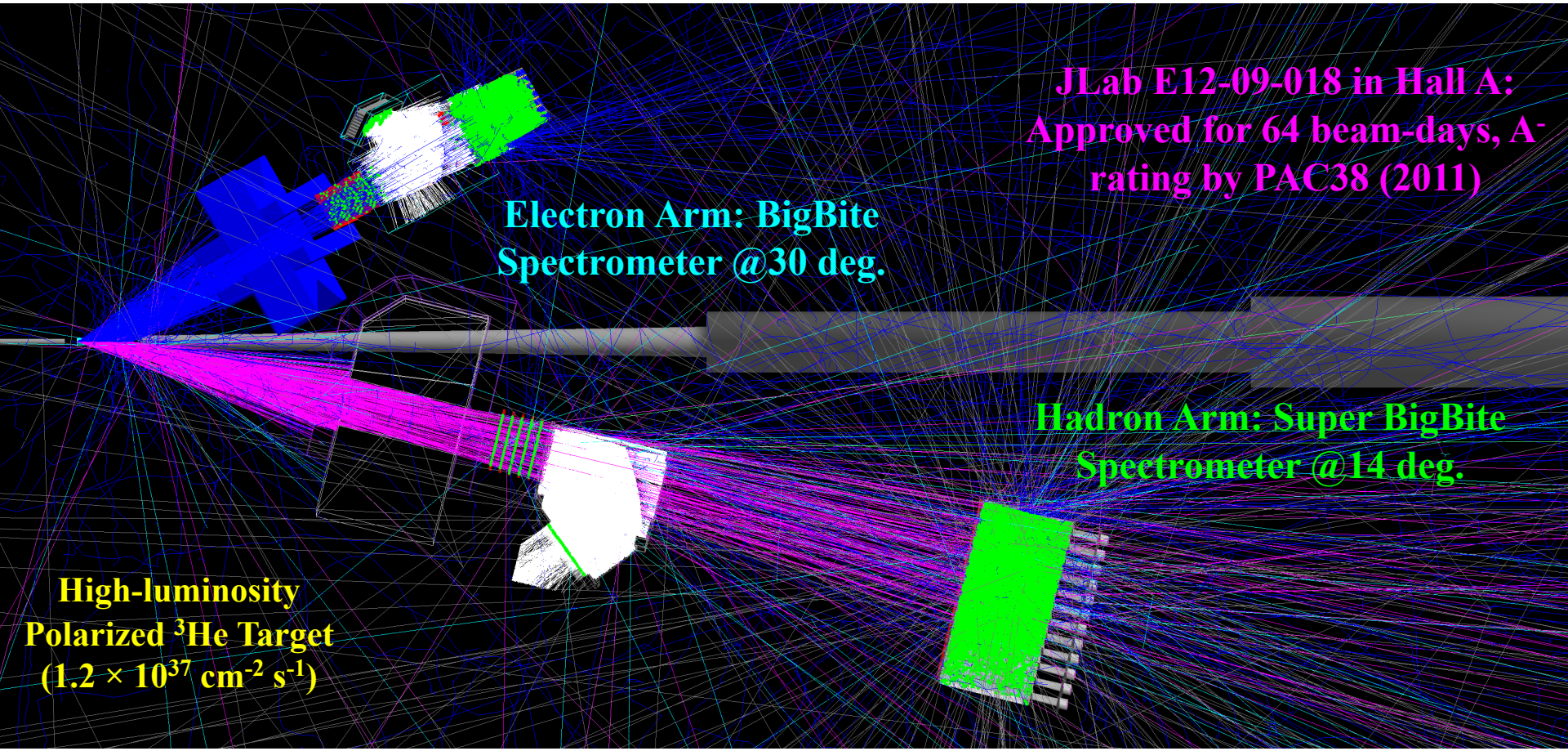

- **E12-09-018** in Hall A: transverse spin physics with high-luminosity polarized ^{3}He.
- 40 (20) days production at E = 11 (8.8) GeV—significant Q^2 range at fixed x
- Collins, Sivers, Pretzelosity, A_{LT} for n(e,e'h)X, h = $\pi^+/\pi^-/\pi^0/K^+/K^-$
- Re-use HERMES RICH detector for charged hadron PID
- Reach high x (up to ~0.7) and high statistical FOM (~1,000X Hall A E06-010 @6 GeV)

SIDIS Kinematic Coverage in E12-09-018

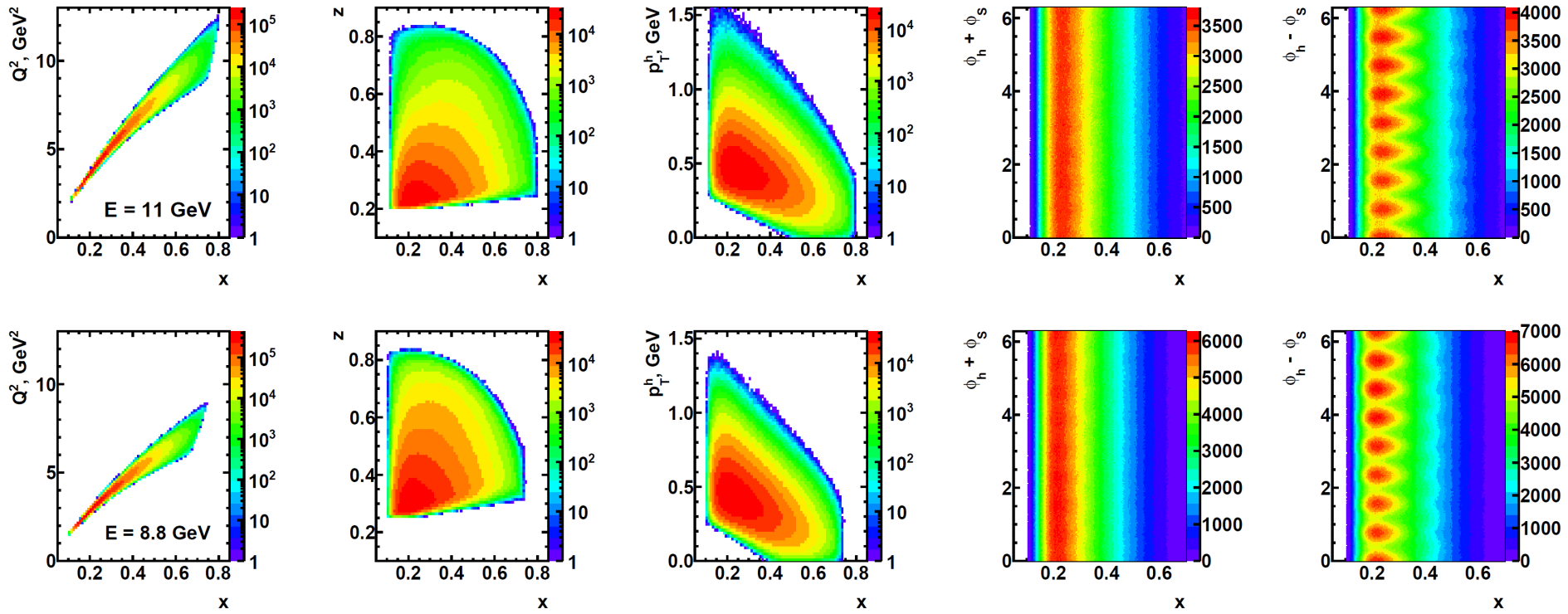

- Wide, independent coverage of x, z, p_T, $\phi_h \pm \phi_S$ in a single spectrometer configuration.
- At least four (preferably 8) target spin directions to achieve full ϕ_S coverage
- Q^2, x strongly correlated due to dimensions of BigBite magnet gap.
- Data at E = 11, 8.8 GeV provide data for significantly different Q^2 at same x
- Systematics control → independent spectrometers, detectors in field-free regions, straight-line tracking, simple, well-defined (but adequately large) acceptance, etc.

SBS+BB Projected Results: Collins and Sivers SSAs

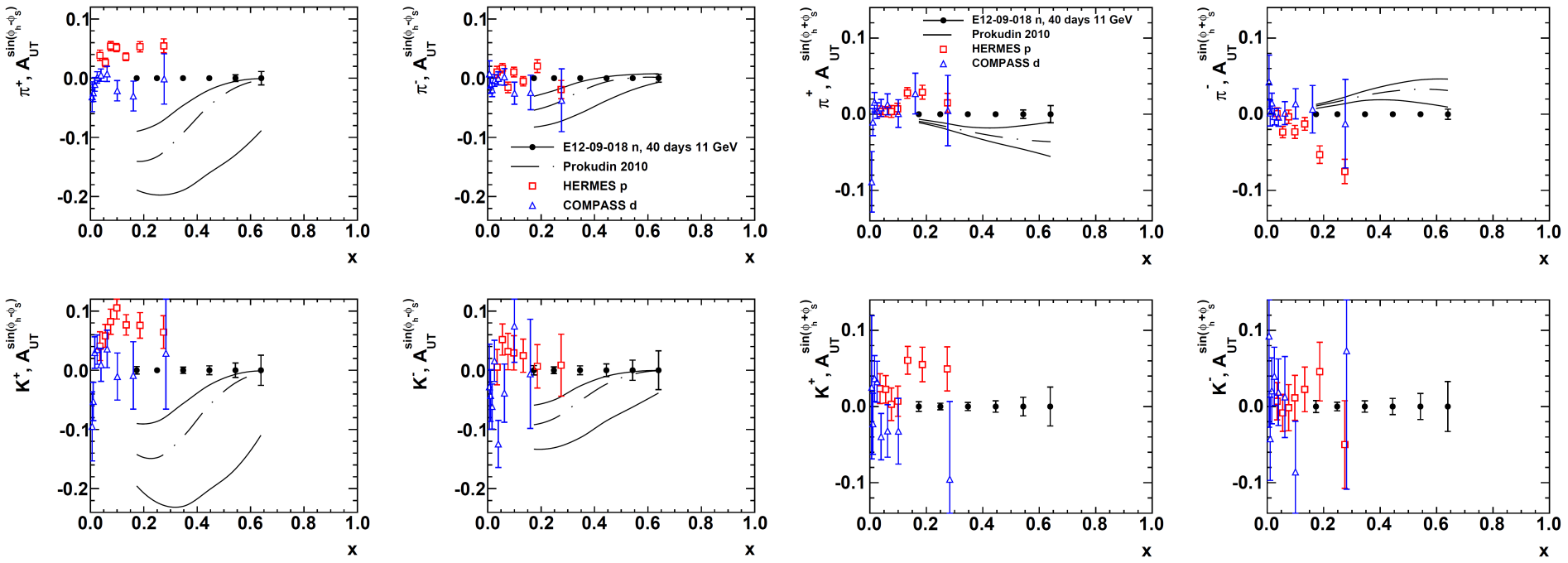

Projected neutron A_{UT}^{Sivers} vs. x (11 GeV data only)

Projected neutron $A_{UT}^{Collins}$ vs. x (11 GeV data only)

- E12-09-018 will achieve statistical FOM for the neutron ~100X better than HERMES proton data and ~1000X better than E06-010 neutron data.
- Kaon and neutral pion data will aid flavor decomposition, and understanding of reaction-mechanism effects.

SBS Future Physics Potential

- SBS program adds a powerful complement of equipment and new capabilities to Hall A for medium-acceptance, high-luminosity physics running
- Examples include:
- Tagged DIS and pion structure function (C12-15-006)
- Precision inclusive proton and neutron spin structure to very high "x"—including g_2^n, g_2^p
- Longitudinally polarized SIDIS on neutron and/or proton targets and spin-flavor decomposition
- Exclusive ϕ production
- J/ψ recoil polarization and study of pentaquark properties
- Others?
- Unlikely that experiments other than currently approved program will run near future, but many of these ideas can/should be ready to run in the event of, e.g., delays in MOLLER/SOLID construction

SBS Program Status

- All major detector and other subsystem components exist and are on track for readiness consistent with the projected experiment schedule
- SBS GMN installation will start in 2020 during the planned long accelerator down
- GMN 2021
- GEN(+SIDIS?) 2021-2022
- GEP: 2022-2023 (depending on whether SIDIS goes first)
- Thank you for your attention!

Backup

Dyson-Schwinger Equations, diquark correlations, and zero crossings of G_{Ep}, G_{En}

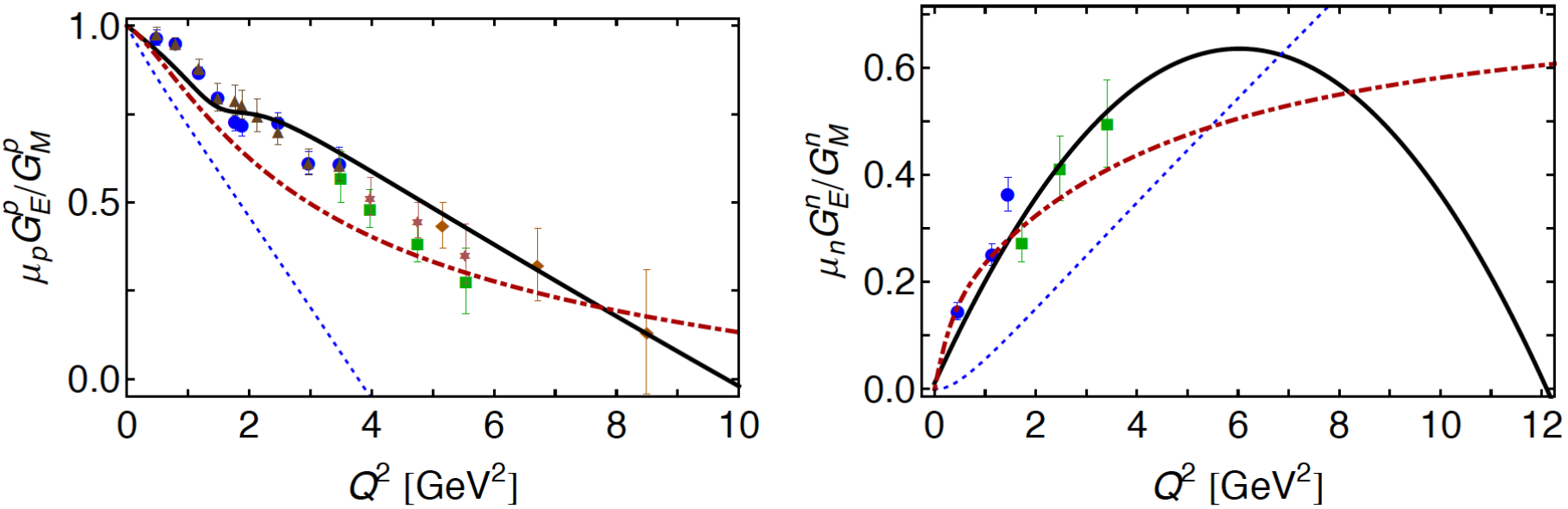

Fig. 3 *Left panel*: normalised ratio of proton electric and magnetic form factors. Curves: *solid, black* – result obtained herein, using our QCD-kindred framework; *Dashed, blue* – CI result [18]; and *dot-dashed, red* – ratio inferred from 2004 parametrisation of experimental data [65]. Data: blue circles [68]; green squares [69]; brown triangles [70]; purple asterisk [71]; and orange diamonds [72]. *Right panel*: normalised ratio of neutron electric and magnetic form factors. Curves: same as in left panel. Data: blue circles [73]; and green squares [74].

J. Segovia, I. Cloet and C. Roberts: Few-Body Syst. 55, 1185 (2014)

Quote from the abstract:

of dynamical chiral symmetry breaking in the bound-state problem. Amongst the results we describe, the following are of particular interest: $G_E^p(Q^2)/G_M^p(Q^2)$ possesses a zero at $Q^2 = 9.5\,\mathrm{GeV}^2$; any change in the interaction which shifts a zero in the proton ratio to larger Q^2 relocates a zero in $G_E^n(Q^2)/G_M^n(Q^2)$ to smaller Q^2; there is likely a value of momentum transfer above which $G_E^n > G_E^p$; and the presence of strong diquark correlations within the nucleon is sufficient to understand empirical extractions of the flavour-separated form factors. Regarding the $\Delta(1232)$-baryon, we find that, *inter*

Elastic *eN* scattering and form factors: formalism

$$\mathcal{M} = \frac{4\pi\alpha}{q^2}\bar{u}(k')\gamma^\mu u(k) g_{\mu\nu}\bar{u}(p')\left[F_1(q^2)\gamma^\nu + F_2(q^2)\frac{i\sigma^{\nu\alpha}q_\alpha}{2M}\right]u(p)$$

Invariant amplitude for elastic eN scattering in the one-photon-exchange approximation

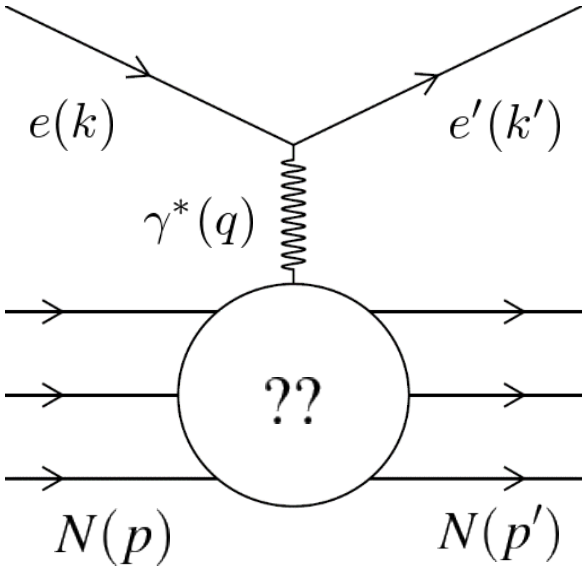

- The most general possible form of the virtual photon-nucleon vertex consistent with Lorentz invariance, parity conservation and gauge invariance is described by two form factors F_1 (Dirac) and F_2 (Pauli):
  - F_1 describes the helicity-conserving amplitude (charge and Dirac magnetic moment)
  - F_2 describes the helicity-flip amplitude (anomalous magnetic moment contribution)

$$G_E \equiv F_1 - \tau F_2$$
$$G_M \equiv F_1 + F_2$$
$$\tau \equiv \frac{Q^2}{4M^2}$$

Sachs Form Factors G_E (electric) and G_M (magnetic), are experimentally convenient linearly independent combinations of F_1, F_2

$$\frac{d\sigma}{d\Omega_e} = \frac{4\alpha^2 {E'_e}^2 \cos^2\frac{\theta_e}{2}}{Q^4}\left(\frac{E'_e}{E_e}\right)\left[\frac{\epsilon G_E^2 + \tau G_M^2}{\epsilon(1+\tau)}\right]$$

$$\epsilon^{-1} = 1 + 2(1+\tau)\tan^2\left(\frac{\theta_e}{2}\right)$$

Differential cross section in the nucleon rest frame:
Rosenbluth formula

$$\sigma_R \equiv \frac{\varepsilon(1+\tau)\frac{d\sigma}{d\Omega_e}}{\left(\frac{d\sigma}{d\Omega_e}\right)_{Mott}} = \varepsilon G_E^2 + \tau G_M^2$$

Rosenbluth Separation Method: Measure cross section at fixed Q^2 as a function of ε to obtain G_E^2 (slope) and G_M^2 (intercept).

Rosenbluth Separation Method

- The nucleon structure-dependent part of the cross section factorizes from the "point-like" part.
- The "reduced cross section" σ_R depends linearly on ϵ for a given Q^2, with slope G_E^2 and intercept τG_M^2.
- Experimentally, one measures $d\sigma/d\Omega$ while varying the beam energy and scattering angle to change ϵ while holding Q^2 constant

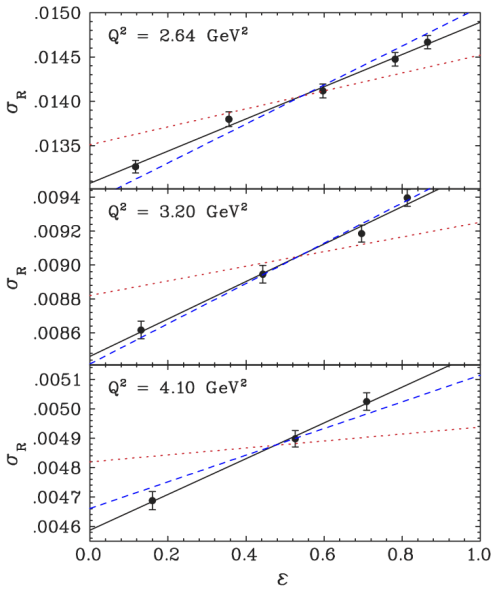

FIG. 2 (color online). Reduced cross sections as a function of ε. The solid line is a linear fit to the reduced cross sections, the dashed line shows the slope expected from scaling ($\mu_p G_E/G_M = 1$), and the dotted line shows the slope predicted by the polarization transfer experiments [6].

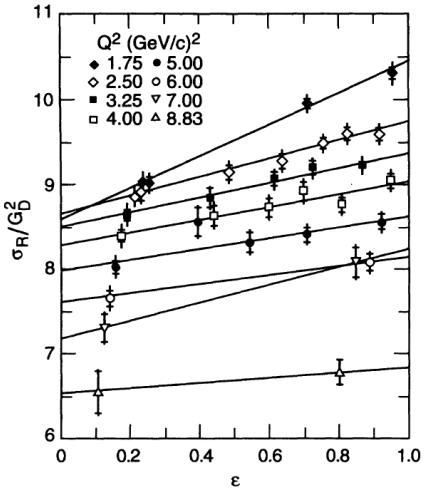

FIG. 22. Reduced cross sections divided by the square of the dipole fit plotted versus ϵ for each value of Q^2. The 1.6 GeV data points correspond to the leftmost point on each line, and the E136 data point is the rightmost point on the $Q^2 = 8.83$ (GeV/c)^2 line. The inner error bars show the statistical error, while the outer error bars show the total point-to-point uncertainty, given by the quadrature sum of the statistical and point-to-point systematic errors. An overall normalization uncertainty of ±1.77% has not been included.

Qattan *et al.*, **Phys. Rev. Lett.** 94, 142301 (2005)

Andivahis *et al.*, **Phys. Rev. D** 50, 5491 (1994)

$$\frac{d\sigma}{d\Omega_e} = \left(\frac{d\sigma}{d\Omega_e}\right)_{Mott} \frac{\epsilon G_E^2 + \tau G_M^2}{\epsilon(1+\tau)}$$

$$\left(\frac{d\sigma}{d\Omega_e}\right)_{Mott} = \frac{\alpha^2 \cos^2\left(\frac{\theta_e}{2}\right)}{4E_e^2 \sin^4\left(\frac{\theta_e}{2}\right)} \frac{E_e'}{E_e}$$

$$\sigma_R = \epsilon G_E^2 + \tau G_M^2$$

$$\tau \equiv \frac{Q^2}{4M_p^2}$$

$$\epsilon \equiv \left[1 + 2(1+\tau)\tan^2\left(\frac{\theta_e}{2}\right)\right]^{-1}$$

Polarization Transfer in Elastic *eN* scattering

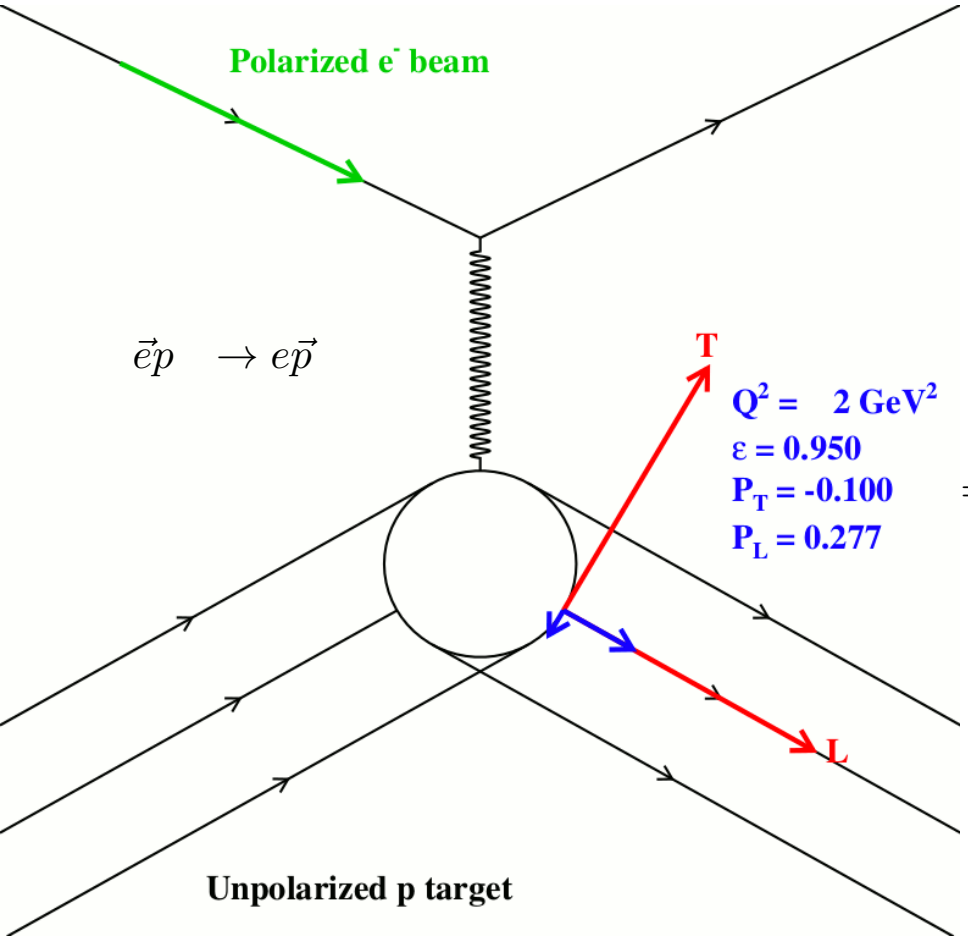

$$P_t = -P_{beam}\sqrt{\frac{2\epsilon(1-\epsilon)}{\tau}}\frac{r}{1+\frac{\epsilon}{\tau}r^2}$$

$$P_\ell = P_{beam}\frac{\sqrt{1-\epsilon^2}}{1+\frac{\epsilon}{\tau}r^2}$$

$$P_n = 0$$

$$r \equiv \frac{G_E}{G_M}$$

$$\Longrightarrow R_p \equiv \mu_p\frac{G_E^p}{G_M^p} = -\mu_p\sqrt{\frac{\tau(1+\epsilon)}{2\epsilon}}\frac{P_t}{P_\ell}$$

- ***The ratio of transferred polarization components is directly proportional to G_E/G_M, and therefore much more sensitive to G_E at large Q^2 than the cross section***

- The polarization transferred to the recoiling proton in the elastic scattering of longitudinally polarized electrons by unpolarized target protons has nonzero components parallel and perpendicular to the momentum transfer in the scattering plane.
- The transferred polarization components provide enhanced sensitivity to the electric (magnetic) form factor at large (small) Q^2.
- A simultaneous measurement of both components in a proton polarimeter allows a precise determination of the ratio of form factors in a single kinematic setting, and provides exact cancellations of many systematic uncertainties, such as acceptance/efficiency, polarimeter instrumental asymmetry and analyzing power, beam polarization, etc., making the method both statistically precise and systematically robust.
- Rapidly falling elastic *ep* cross section and polarimeter figure-of-merit at large Q^2 necessitate high luminosity, high duty-cycle, and large acceptance. Such measurements can only presently be performed using CEBAF@JLab.

Polarized Beam-Polarized Target Asymmetry

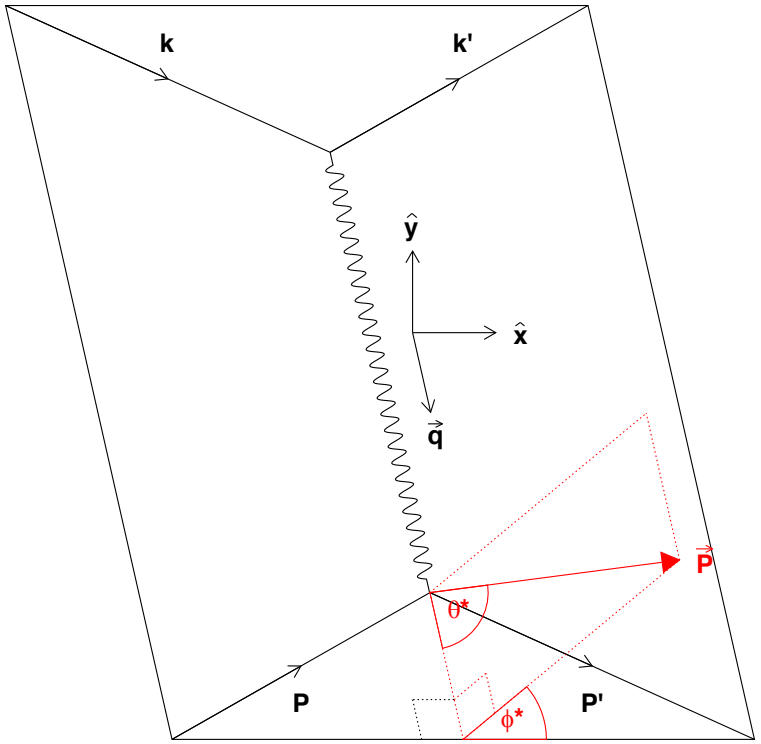

- The beam helicity asymmetry in elastic *eN* scattering from a polarized target is related to the transferred polarization by time reversal symmetry.
- The asymmetry A_t for target polarization perpendicular to the momentum transfer but parallel to the scattering plane ($\theta^* = 90°, \phi^* = 0$) equals the transverse component P_t of the transferred polarization.
- The asymmetry A_ℓ for target polarization along the momentum transfer direction ($\theta^* = 0$) is equal in magnitude but opposite in sign to the longitudinal transferred polarization P_ℓ.
- The sign change between A_ℓ and P_ℓ is due to the proton spin flip required for the absorption of the transversely polarized virtual photon

$\vec{\mathbf{P}}$ $\equiv$ Target polarization

$$
\begin{aligned}
A_{eN} &= -\frac{P_{beam}P_{target}}{1+\frac{\epsilon}{\tau}r^2}\left[\left(\sqrt{\frac{2\epsilon(1-\epsilon)}{\tau}}\sin\theta^*\cos\phi^*\right)r+\sqrt{1-\epsilon^2}\cos\theta^*\right] \\
&\equiv P_{target}\left[A_t\sin\theta^*\cos\phi^*+A_\ell\cos\theta^*\right] \\
A_t &= P_t \\
A_\ell &= -P_\ell \\
A_n &= P_n = 0
\end{aligned}
$$

Mapping the transverse densities and nucleon Imaging, I

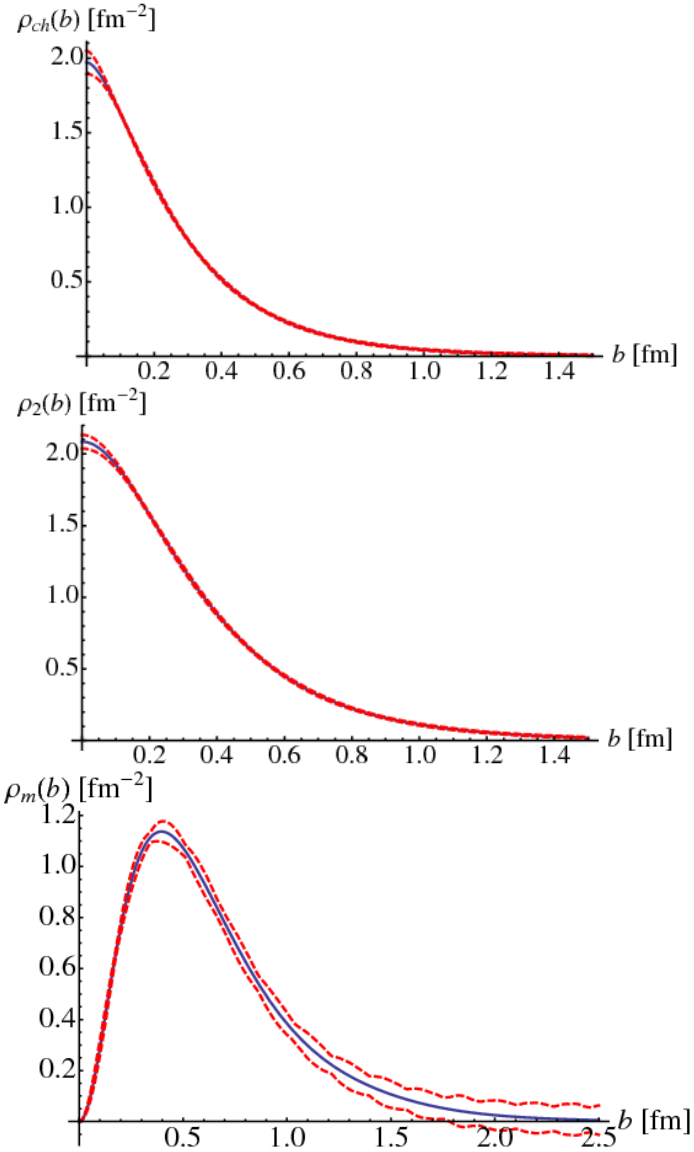

- Miller et al, **Phys. Rev. C, 83, 015203 (2011)**: ***model-independent,*** impact parameter-space charge and magnetization densities in the infinite momentum frame.
- Proton results shown for
  - Charge
  - 2D Fourier transform of F_2 (Pauli FF)
  - Anomalous magnetization density

$$\rho_{ch}(b) = \frac{1}{2\pi}\int QdQJ_0(Qb)F_1(Q^2)$$

$$\rho_2(b) = \frac{1}{2\pi}\int QdQJ_0(Qb)F_2(Q^2)$$

$$\rho_m(b) = -b\frac{d}{db}\rho_2(b) = \frac{b}{2\pi}\int Q^2dQJ_1(Qb)F_2(Q^2)$$